Proceedings Paper:
Etarhouni, M, Chong, B and Zhang, L (2021) Series-Parallel Differential Power Processing Scheme for Maximised Power Extraction from Mismatched Photovoltaic Panels. In: Proceedings of the 10th International Conference on Power Electronics, Machines and Drives (PEMD 2020). The 10th International Conference on Power Electronics, Machines and Drives (PEMD 2020), 15-17 Dec 2020, Nottingham, UK. IEEE , pp. 814-819. ISBN 978-1-83953-542-0

https://doi.org/10.1049/icp.2021.0997

Series-Parallel Differential Power Processing Scheme for Maximised Power Extraction from Mismatched Photovoltaic Panels

Mohamed Etarhouni*, Benjamin Chong, Li Zhang

*School of Electronic & Electrical Engineering, University of Leeds, Leeds, UK, *fy09mse@leeds.ac.uk*

Keywords: Photovoltaic (PV) array, Partial Shading Conditions (PSCs), Optimal Power, Differential Power Processing (DPP), Maximum Power Point Tracking (MPPT)

Abstract

In recent years, there has been an increasing interest in utilising Differential Power Processing converters (DPP) in Photovoltaic (PV) applications to achieve the maximum power point tracking (MPPT), minimum losses and high efficiency under unequal lighting conditions. This paper presents a novel Series and Parallel (SP) DPP converters scheme, with a proper control technique to optimise the system output power under mismatch conditions compared to that of a conventional 2×2 SP array which is protected with bypass diodes. The simulation results of such system show significant improvements in the total power of the SP-DPP system under PSCs.

1 Introduction

Power converters have been used in extracting the maximum power from photovoltaic (PV) arrays containing modules which are mismatched, mainly due to partial shading and manufacturing variations. One of the many proposed schemes is the module Integrated Converter (MIC), using DC-DC converters with each connected to a single PV module or string of modules. The converter outputs can be combined in series-parallel, which, with proper control, enables the converter to process all the available power. All the power from a module passes through its associated converter, which is therefore known as a Full Power Processing (FPP) converter or DC optimise [1]. One of the main disadvantages evaluated by authors in [1, 2] is that different shading conditions encountered by the chained PV modules may lead to some modules not able to operates in their optimal (i.e. MPP) operation states.

A different scheme uses so-called Differential Power Processing (DPP) converters; these allow maximum power point tracking (MPPT) for the independent PV modules, but each processes only part of a module's extracted power. Compared to the MIC scheme described above, the DPP has lower voltage and current ratings of power switching devices, reduced size and overall system cost [3]. DPP converter topologies can be classified into series and parallel schemes. Many existing research papers treat the series scheme where converters are embedded within the series string of PV panels [4]. The work has led the system to achieve MPP operation for all modules and is similar to the MIC scheme. However, under a very large difference in solar irradiations, the series DPP must process a significant amount of power for MPP operation, hence reduces the efficiency and this becomes a limitation [3]. On the other hand, the voltage across each individual series DPP string may be different, when these strings are connected in parallel to a DC-bus, the differences in voltage may prevent some strings from generating their maximum power, or in bad cases, any power.
A parallel DPP can potentially address this shortcoming, and several parallel topologies have been reported [5-7]. They involve either direct or indirect connections between two PV panels. The former may be implemented, for example, by interconnecting PV panels via a bidirectional flyback or Sepic converter [6-7]. For indirect connection, a frond-end converter such as an inverted buck can be placed between the DC bus and DPP converter [5]. The work of [7] has validated the superiority of both these types of DPP configuration among all other topologies, including MICs and series DPP layouts. The main advantage of parallel DPP over the series-connected type is that the voltage characteristics under this DPP topology are relatively unchanged by extreme differences in irradiation, compared to the series DPP connection [5, 6]. However, the operating DC output terminal voltage is much lower than that of the series DPP. Apart from this existing research on either series or parallel DPP schemes, no studies have been found which combine them in an integrated Series-Parallel (SP) DPP configuration for a PV array.

This paper presents a novel scheme for a combined Series and Parallel (SP) DPP converter, as seen in Fig. 1(b), together with its control strategy for 2×2 PV array, to raise the system's generated output power under unequal light levels. The paper also illustrates the overall principle of this system, the mathematical model, and MPP control schemes. The first implementation was based on a PI controller, leading to fast steady-state response with minimum overshoot, where the derived transfer function of the inner BCCs was used to tune the controller parameters. Then, the well-known Perturb-Observe (P&O) MPPT scheme has been implemented for both the inner BCCs and outer DPPs. The P&O algorithm for this PV system predicts the MPPT voltages for the four PV modules within the SP DPP system under their respective weather conditions.

Simulation results are shown here which verify the effectiveness of the SP DPP structure in Fig. 1(b) in terms of the generated power, and the results are compared to those of the conventional PV array protected with bypass diodes, as seen in Fig. 1(a).

2. Configuration of The SP-DPP System

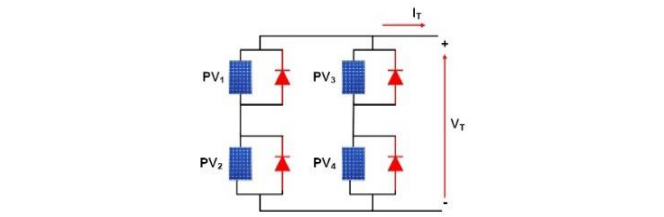

(a)

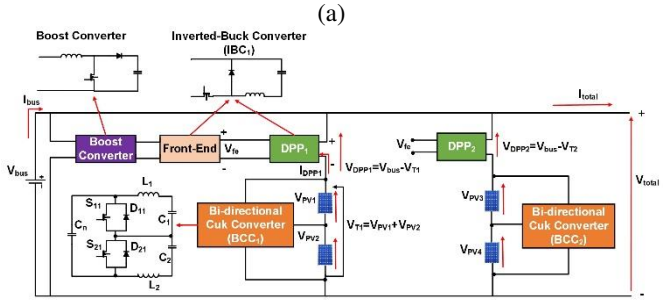

(b)

Fig. 1(a) 2×2 SP PV array (b) SP configuration of parallel DPP converters for 2×2 PV array

The proposed DPP system is as shown in Fig. 1(b). It consists of two series DPP converter-PV units each comprising a Bidirectional Cuk Converter (BCC), and with its three terminals pairs connected to two series-connected PV panels(i.e. PV_1 and PV_2 for BCC_1, PV_3 and PV_4 for BCC_2). Then, the two such configurations are connected in parallel with a set of DPP converters, which are primarily implemented based on a lower-switch buck converter for high efficiency and compactness [5].

2.1 Operating Principles of BCCs With Cascaded PV Units

As seen in Fig. 1(b), the main advantage of having BCCs for each series string is that this type of converter provides continuous input and output currents and thus require smaller capacitors compared to other suitable converters such as those based on buck-boost [3]. BCCs allow bidirectional current and power flow and can be controlled to enable either panels to produce higher power. The operating principles of this converter scheme are illustrated in detail in an earlier paper [8]. In summary, the inner BCC is utilised to regulate the voltage ratio of the two serially-linked PV modules.

There are two main operating modes existing with this system; mode 1 is when the solar intensity levels received by the two panels (in either string) are similar. In this mode, the PV panels of that string ideally generate the same currents and powers. The BCC of that string is idle and completely switched off, so absorbs negligible power. For mode 2 where the irradiations on both modules are different, i.e. partial shading occurs for the PV panels connected to a BCC, their voltages are different. Under this condition, the relevant BCC needs to be activated in order to provide a path for the differential PV current. With only two PV panels connected to a BCC, and two switch-diode pairs available, they are selected according to the differences in light intensity and their duty ratios are determined as follows [8]:

Case (1), when $G_1 > G_2$, S_{11}-D_{21} active, $\frac{V_{PV2}}{V_{PV1}} = \frac{K_{11}}{1-K_{21}}$

Case (2), when $G_2 > G_1$, S_{21}-D_{11} active, $\frac{V_{PV1}}{V_{PV2}} = \frac{K_{21}}{1-K_{21}}$

where V_{PV1} and V_{PV2} are the terminal voltages of PV_1 and PV_2 modules respectively, G_1 and G_2 are solar irradiations received by PV_1 and PV_2 while K_{11} and K_{21} are the duty ratios associated with S_{11} and S_{21} respectively, as seen in Fig. 1(b). The output of the BCC converter is connected in parallel with the DPP converter scheme in this work. Hence, the DPP converter ensures the global MPP tracking (GMPP), where the sum of the PV voltages is at MPP.

2.2 Operating Principles of Parallel DPP Converters

As shown in Fig 1(b), there is a DPP converter connected in series between the DC bus and each PV-BCC unit, forming a series string, and several such strings (two here for clarity) are wired in parallel.Thus this configuration is named the series-parallel (SP) DPP scheme.There is a single boost and a single Front-End converter feeding all the inputs of the DPP converters. The initial boost converter is used as a power conditioner. The Front-End and DPPs converters are implemented as Inverted-Buck Converters (IBC). An IBC scheme was also introduced in [6-7].

Assuming the MPP has been reached for every PV panel, the duty cycle of each BCC is determined by the *ratio* of the MPP voltages of its two associated panels. However, the total voltage across each PV string must also equal the sum of the MPP voltages of its panels, and this will usually differ from string to string. Hence to allow the strings to be connected in parallel to a common bus, the total voltage of each string must be changed, which is achieved in the scheme shown here by applying a variable additive offset to it. This is the function of the parallel DPP converter connected in series with each string.

As seen in Fig. 1(b), the output voltage of the Front-End converter (V_{fe}) is applied to the inputs of both DPP converters (DPP_1 and DPP_2). The primary function of the front-end converter is to reduce the bus voltage (V_{bus}) to an intermediate voltage level (V_{fe}), thus avoiding too low duty ratios for each of the DPP converters. The discussion here assumes the Front-End converter output voltage V_{fe} is kept constant, as is convenient but not in principle essential. Under unequal irradiation conditions, the PV-BCC units are now active depending on the difference between irradiation levels of the modules as mentioned earlier. Then, each BCC unit supplies its total current and voltage to the corresponding parallel DPP schemes,including DPP_1 and DPP_2 as applicable.

2.2.1 Power Loss Analysis of DPP converters: DPP converters are recently receiving significant attention in renewable energy applications since they process partial power under PSCs comparing to MICs and FPP topologies, thus resulting in small power losses and improved total system efficiency. For the SP-DPP system in Fig. 1(b), the PV-BCC unit and bus voltages are related by the following expression [5, 7]:

$$V_{bus} = V_{Tn} + V_{DPPn} \quad (1)$$

Thus, the terminal current of the overall DPP system shown above, I_T can also be obtained as follows:

$$I_T = \sum_{i=1}^{K} \frac{V_{Tn}}{V_{bus}} \times I_{Tn} \quad (2)$$

For n = 1, 2, ……., k. The total power generated by parallel DPP converters is determined as:

$$P_{DPP} = \sum_{i=1}^{K} (V_{bus} - V_{Tn}) \times I_{Tn} \quad (3)$$

Equation (3) shows that if the bus voltage is similar to that of each PV-BCC units, the total power of the DPP converters is decreased as well as the power loss in the DPP scheme. Generally, the power loss in FPP converter topologies is given as [5]:

$$P_{loss\,(FPP)} = V_{MPP} \times I_{MPP} \times (1 - \eta_{Conv}) \quad (4)$$

Where V_{MPP}, I_{MPP} are the operating points of the I-V curve of a PV module under certain irradiation level. η_{Conv} is the efficiency of the DC-DC converter considered in FPP topology. For the total SP-DPP system in Fig. 1(b), the total power loss of this system, including the Front-End converter is written as:

$$P_{Loss\,(SP-DPP)} = \frac{1 - \eta_{FE}}{\eta_{FE} \times \eta_{Conv}} \sum_{i=1}^{K} (V_{bus} - V_{Tn}) \times I_{Tn} \quad (5)$$

Where η_{FE} is the Front-End converter efficiency. By examining equation (5), it can be established that introducing the proposed system in Fig. 1(b) minimises the total power loss due to the voltage difference facilitated by this configuration. However, using either bypass diodes shown in Fig. 1(a) or conventional FPP schemes existing in the literature, can result in more power losses than that of the SP-DPP system, as seen in equation (4).

3. Model-Based Control Scheme of the SP-DPP System for MPP Tracking

The main challenge for implementing a robust controller is that, since each of the inner BCCs has two input-output ends connected to PV panels, voltage regulation would be needed across both terminal ends in such a case [8]. The key objective of a system controller is to enable all PV panels in parallel strings in the system shown in Fig. 1(b) to operate at their respective MPP under any weather conditions. Therefore, Fig. 2 shows the control scheme for the SP-DPP system, which consists of two inner BCC converters along with two outer DPP converters in addition to one Front-End converter. Thus, these converters requires a coordinated control to achieve the optimal performance.

3.1. Transfer Function of PV-BCC Model

This is now derived, as required for optimising the control loop parameters. The derivation assumes that the irradiation received by PV_1 is higher than that of PV_2; thus, S_{11}-D_{21} is active. The alternate case follows from the left-right symmetry of the BCC. Continuous Conduction Mode (CCM) is assumed.The standard state-space variable vector x is used to describe the dynamics of the BCC in 'on' and 'off' operating modes. Therefore, a combination of the obtained equations leads to a model of the BCC averaged over a switching interval. Then, by applying a small ac signal analysis to all state variables associated with the averaged equation, and finding their laplace transform, the transfer function between the rate of changes of PV voltages to the switch duty ratio is expressed as [8]:

$$G_1(s) = \frac{\hat{v}_{pv1}(s)}{\hat{k}_1(s)} = \frac{b_3 s^3 + b_2 s^2 + b_1 s + b_0}{a_5 s^5 + a_4 s^4 + a_3 s^3 + a_2 s^2 + a_1 s + a_0} V_T \quad (6)$$

$$G_2(s) = \frac{\hat{v}_{pv2}(s)}{\hat{k}_1(s)} = \frac{d_3 s^3 + d_2 s^2 + d_1 s + d_0}{a_5 s^5 + a_4 s^4 + a_3 s^3 + a_2 s^2 + a_1 s + a_0} V_T \quad (7)$$

where the coefficients are given by expressions listed in Appendix 1.

3.2 Voltage-Feeddback Control of BCC & DPP converters

Referring to the measured solar intensity levels and the shading condition within the four panels, the switching scheme of the inner BCCs can be selected as seen in sub-section 2.1. The switch duty ratio can be subsequently set to vary the terminal voltage across each PV module within the BCC units based on their corresponding MPP. Whilst setting the operating modes for inner BCCs, the terminal voltage of the total SP-DPP system (V_{total}) can be regulated by controlling DPPs and Front-End converters to find the optimal overall power output.

The input voltage variations from its desired level is considered as the disturbance to the output, thus they have to be minimised. Therefore, the PI control formulae below clearly presents the subtraction between the input voltage errors and both the proportional and integration terms. The switch duty ratio of the two BCCs are then evaluated following the PI algorithm:

$$K_{11} = K_{P1} \times [(V_{PV2}^{*} - V_{PV2}^{m}) - (V_{PV1}^{*} - V_{PV1}^{m})] + K_{I1} \times [(V_{PV2}^{*} - V_{PV2}^{m}) - (V_{PV1}^{*} - V_{PV1}^{m})] \quad (8)$$

$$K_{21} = 1 - K_{11} \quad (9)$$

$$K_{22} = K_{P2} \times [(V_{PV4}^{*} - V_{PV4}^{m}) - (V_{PV3}^{*} - V_{PV3}^{m})] + K_{I2} \times [(V_{PV4}^{*} - V_{PV4}^{m}) - (V_{PV3}^{*} - V_{PV3}^{m})] \quad (10)$$

$$K_{12} = 1 - K_{22} \quad (11)$$

Where $V_{PV1}^{m}, V_{PV2}^{m}, V_{PV3}^{m}, V_{PV4}^{m}$ are the measured PV voltages, as shown in Fig. 2, and V_{PV1}^{*}, V_{PV2}^{*}, V_{PV3}^{*}, V_{PV4}^{*} are their corresponding desired values. K_{11} and K_{21} are the duty ratios used for BCC_1 switches, while K_{22} and K_{12} are used to control BCC_2 swithces. It can also be clear that the PI controller needs information regarding the optimal values of the four PV voltages while setting V_{PV1}^{*}, V_{PV2}^{*}, V_{PV3}^{*} and V_{PV4}^{*}. This was done by creating a PV model for the four PV panels based on the curve-fitting method [9]. This model will estimate the PV voltages, thus enabling the PV modules to generate the maximum global power, then feed them to the associated PI controller loop. Similarly, this procedure continues to control the outer DPP converters. The terminal voltage of each DPP converter is determined by the individual terminal capacitors across each BCC unit, as shown in Fig. 2. The reference voltage for the output of each of the two outer DPP converters is set as the sum of the reference voltages of two PV modules within the individual BCCs units. For example, V_{T1}^{*}, V_{T1}^{m} and V_{T2}^{*}, V_{T2}^{m} are used to regulate the duty ratios K_{DPP1} and K_{DPP2} of the outer DPP converters. The output voltage of the Front-End converter (V_{fe}) is held constant at about 13V by regulating K_{FE}.

Finally, choosing K_{P1}, K_{P2}, K_{I1}, K_{I2} and the remaining proportional and integral gain values used in inner the outer control loops for DPP converters are altogether based on eliminating the steady-state errors in the terminal voltages of each PV module, and achieving a fast and stable dynamic response. The tuning of gain values of PI controllers for inner and outer converters are all included in the next section.

3.3 Perturb and Observe (P&O) MPPT method

The well-known Perturbation and Observation (P&O) algorithm [10, 11] can be alternatively applied in searching the optimal PV

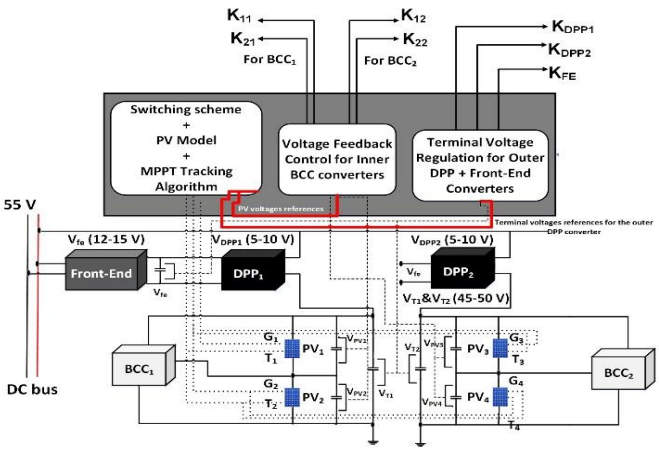

Fig. 2 Configuration of the control scheme for the SP-DPP system

voltages of the SP-DPP system. The P&O algorithm sets PV voltages of all modules to the desired level upon every detection of a change in the solar irradiation conditions; thus, the duty ratio of inner and outer converters are updated accordingly.

With using the P&O algorithm, a computer model is constructed such that its design specifications are similar to those for PV model-based-type. However, the control system is now only based on P&O MATLAB algorithm for MPPT; thus, it is implemented using MATLAB user-defined function block with the associated inputs. Then, this MPPT block is incorporated into the SIMULINK model. This algorithm starts with measuring the PV system power across its terminal ends and compares this power value with the previous one. Therefore, if the PV power is smaller, the algorithm will either decrease or increase the switch duty ratio by a constant amount of 0.001. The flowchart shown in Fig. 3 illustrates the full operating steps of the P&O algorithm used in the simulation work. Since the four PV modules used in the SP-DPP system are all identical, an example of Power-Voltage (P-V) characteristics of a single module is shown in Fig. 4(a). It can be noted that the MPP voltage varies between 25-28 V. Therefore, Fig. 4(b) shows the action of P&O in response to the change of weather conditions.

In the present work, for each variation in duty ratios for switches of the two outer DPP converters (S_{DPP1} & S_{DPP2}), the P&O method tunes that for S_{11} and S_{21} of each BCC unit many times. As S_{DPP1} & S_{DPP2} has a significant impact in searching for the desired power points, the duty ratios of inner BCCs and outer DPPs would track the false MPP without this delay. Therefore, the sampling time used in the P&O method for the inner converters is 1×10^{-5} seconds while that for the outer converters is 0.01 seconds.

4. Simulation Results & Discussions

The above two control schemes were implemented and applied to a simulated SP-DPP system model comprising two inner BCCs along with two outer DPPs, which are linked to the DC bus through a Front-End Converter, as seen in Fig. 2. This system has four identical PV modules (i.e., PV_1, PV_2, PV_3 and PV_4) and two BCCs; BCC_1 is connected between PV_1 and PV_2, while BCC_2 is connected between PV_3 and PV_4. The parameters of the whole SP-DPP system are listed in Table 1. Note that the all inductors and capacitors of the inner BCCs and output DPPs are designed for the current and voltage ripples limited to about 5% of their average values.

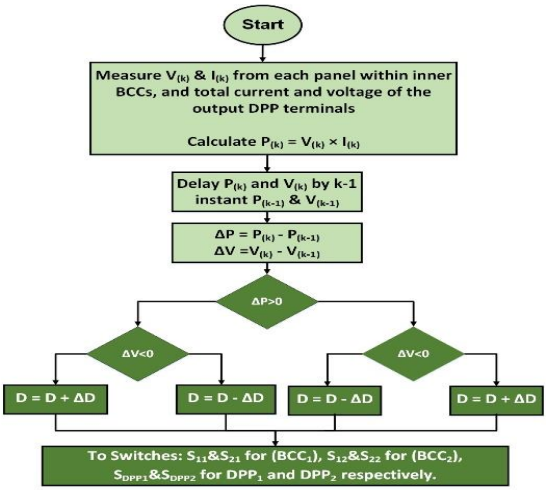

Fig. 3 Flowchart of P&O algorithm used in the SP-DPP system

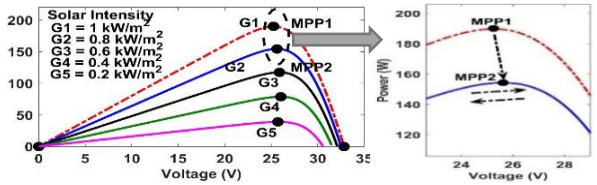

(a) (b)

Fig. 4 (a) P-V characteristics under different irradiance levels (b) The action of P&O in response to weather condition changes

Selecting K_I and K_P values of the control loops for BCCs and DPPs converters was achieved based on fast dynamic response and eliminating the steady-state errors in the terminal voltages of PV modules. In this case, the switching frequency is assumed to be high enough, so that small-signal modelling is still accurate. The sampling time of PI controllers for BCCs and DPPs is carefully matched; thus, the inner controllers for BCCs are at least ten times faster than the outer one for DPPs. The switching frequency used for all converters is 20 kHz. All PV modules are identical, and panel type 'Apollo Solar Energy ASEC-190G6S' was chosen from SIMULINK SimPower tool and considered for the simulation work. The short-circuit current (I_{SC}) and open-circuit voltage (V_{OC}) for this type is given as 6.751A and 32.83V respectively.

To start with, the SP-DPP system was tested using feedback controllers under different weather conditions. Therefore, various solar intensity levels are set over the four PV modules, as seen in Fig. 5 to validate this system model and extract the maximum power available under PSCs. Figs. (6) and (7) respectively depicts the simulation responses of the total system power along with its optimal value, powers and voltages of the individual panels of the SP-DPP system under PSCs. As shown in Fig. 5, modules PV_1 and PV_3 receive full irradiation levels of 1000 W/m^2 while PV_2 and PV_4 are partially shaded at the same level of 800 W/m^2 between 0 and 0.2 seconds. In this case, the created MPP model starts to compute the new values of each panel; hence, S_{11}-D_{21} of both inner BCCs are active.

In contrast, the closed-loop control begins to adjust the duty ratios between the PV voltages based on regulating duty ratios of the inner BCCs. Once these voltage responses start to settle, operating points of the outer DPPs are updated accordingly. After about 0.03

Table 1 Parameters of SP-DPP system used in simulation

Symbol	Parameter	Value
L_1-L_7	Inductors for inner BCCs and outer DPPs	8mH
C_1-C_6	Input and output capacitors for BCC_1&BCC_2	20μF
C_{n1}&C_{n2}	Energy capacitors for BCC_1&BCC_2	10μF
C_7-C_9	Output capacitors C_7 for Front-End, C_8&C_9 for DPP_S	50μF & 20μF
K_{I1}&K_{I2}, K_{P1}&K_{P2}	PI parameters for inner BCCs	10&0.001
K_{I3}&K_{I4}, K_{P3}&K_{P4}	PI parameters for outer DPPs	4&0.5×10^{-6}
K_{I5}&K_{P5}	PI parameters for Front-End	2&0.5×10^{-3}

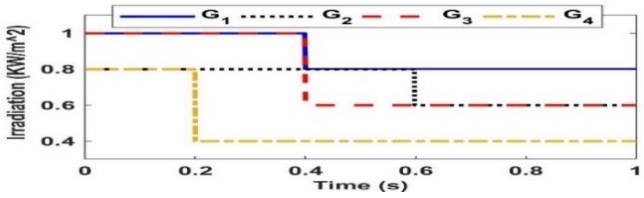

Fig. 5 Solar intensity variation in the simulation model

second, all PV voltages follow their MPP values; thus, the maximum available power can be extracted.

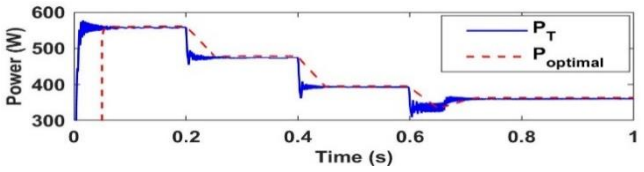

(a)

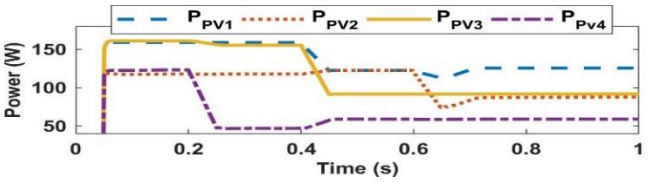

(b)

Fig. 6 Simulated power responses (a) total power delivered to theload and its optimal value (b) power of the individual panels

At 0.2 second, only PV_4 is heavily shaded while the remaining modules remain the same. The control scheme can still lead all PV modules to transition to their new MPP voltages. Terminal voltages of the outer DPPs converters are still regulated as the difference between the DC bus voltage and the terminal voltage of each of the inner BCCs. At 0.4 second, irradiation received by PV_1 falls to a similar level of that on PV_2, however, insolation levels of PV_3 drops slightly, leading to a small voltage overshoot of 0.5 V for PV_4.

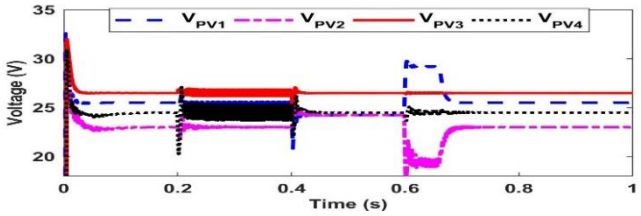

Fig. 7 Simulated voltage responses of the four PV modules

On the other hand, the control system can still enable the SP-DPP system to be stable during this operating period and restore the optimal PV operation. Finally, at 0.6, the solar irradiation received by PV_2 decreases leading to a negligible overshoot of PV_1. Therefore, all the PV voltages settle to their new steady-state values after 0.7893 seconds, as seen in Fig. 7. Table 2 below lists the maximum power available from the PV modules along with the total simulated power by the SP-DPP system under four shading conditions.

Table 2 Maximum power drawn from PV panels and the simulated power using SP-DPP system

Solar Irradiations (KW/m^2)				**Optimal power from PV modules**	**Total power using SP-DPP system**
G_1	**G_2**	**G_3**	**G_4**		
1	0.8	1	0.8	561.4 W	560.1 W
1	0.8	1	0.4	479.4 W	476.6 W
0.8	0.8	0.6	0.4	395.5 W	394.6 W
0.8	0.6	0.6	0.4	363.6 W	361.8 W

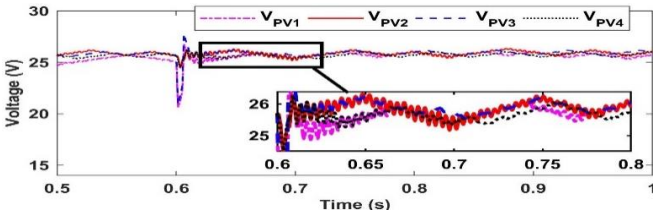

Fig. 8 Simulated PV voltages using P&O based control

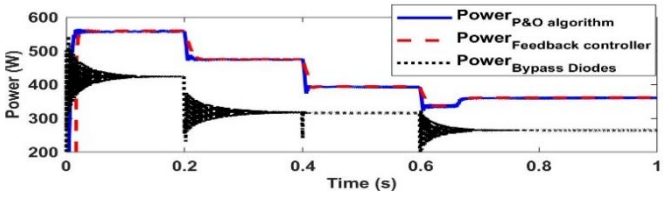

Fig. 9 Comparison between the extracted total power using Feedback controller, bypass diodes and that using P&O control

As mentioned in the previous section, the P&O tracking algorithm was implemented and applied to the SP-DPP model to extract the maximum available power. Before using the P&O method, all PV voltages are set as equal; thus, the duty ratios of the inner BCCs are set as 0.5. The sampling time for the BCCs is 1×10^{-5}s and 0.01s for the DPPs. Fig. 8 demonstrates the simulated PV voltages under the same irradiance variations shown in Fig. 5 above. When comparing to the feedback-control scheme, Fig. 8 shows more oscillations in the voltage responses, since the P&O continuously determines the best duty cycle value for MPPT. There can also be seen that PV voltages have large overshoots at 0.6 seconds when

PV_2 experiences a significant step change, this is because the predicted MPP voltages from P&O method are directly used to regulate the duty cycle ratio of the converter. It is noted that responses of all PV voltages take an average time of 0.091 seconds to settle down to a steady-state value.

Fig. 9 shows a comparison between the performance of SP-DPP system to the conventional method using bypass diodes, as seen in Fig. 1(a). Therefore, the traditional 2×2 PV array system above was simulated with a simple boost converter connected across its terminal ends. Thus, the extracted total power of this system was compared to that of the SP-DPP system using both feedback controller and P&O algorithm-based control under shading conditions in Fig. 5. Hence, Table 3 shows a significant improvement of the overall extracted power from SP-DPP system using feedback control by about **40.02%** and **36.43%** compared to that using bypass diodes (P_D) under cases 2 and 4 respectively in the variations of solar irradiation.

Table 3 Maximum power available by PV modules and power generated by SP-DPP system using two control methods

Solar Irradiations (KW/m^2)				**$P_{SP\text{-}DPP}$ (Feedback)**	**$P_{SP\text{-}DPP}$ (P&O)**	**P_D**
G_1	**G_2**	**G_3**	**G_4**			
1	0.8	1	0.8	**560.1W**	558.6W	424.8W
1	0.8	1	0.4	**476.6W**	474.8W	340.3W
0.8	0.8	0.6	0.4	**394.6W**	393W	316.5W
0.8	0.6	0.6	0.4	**361.8W**	360.5W	265.2W

5 Conclusion

A practical PV array usually has to contain series connected strings of modules, with strings further interconnected in parallel. Maximum power point tracking throughout the array requires adjustment of both module currents and string voltages.

This work has established the viability of a maximum power point tracking system in which both adjustments are performed in a differential power processing mode, the first using bidirectional Cuk converters and the second using inverted buck converters. A single front end converter of two stages was also used. Accurate control has been demonstrated using both model-based and Perturb-and-Observe schemes, and high overall efficiency was found to be achievable, with total output power within 1% of the theoretical maximum for the given modules and light conditions.

6 References

[1] Olalla, C.; Maksimovic, D.; Deline, C.; Martinez-Salamero, L. Impact of Distributed Power Electronics on the Lifetime and Reliability of PV Systems. Prog. Photovolt. Res. Appl. 2017, 25, 821–835.

[2] S. Maity and P. K. Sahu, "Modeling and Analysis of a Fast and Robust Module-Integrated Analog Photovoltaic MPP Tracker," IEEE Transactions on Power Electronics, vol. 31, pp. 280-291, 2016.

[3] Y. Jeon, H. Lee, K. A. Kim, and J. Park, "Least Power Point Tracking Method for Photovoltaic Differential Power Processing Systems," IEEE Transactions on Power Electronics, vol. 32, pp. 1941-1951, 2017.

[4] Y. Jeon and J. Park, "Unit-Minimum Least Power Point Tracking for the Optimization of Photovoltaic Differential Power Processing Systems," IEEE Transactions on Power Electronics, vol. 34, pp. 311-324, 2019.

[5] H. Lee and K. A. Kim, "Design Considerations for Parallel Differential Power Processing Converters in a Photovoltaic-Powered Wearable Application," Energies, vol. 11, pp. 1-17, 2018.

[6] F. S. Bagci, Y. Liu, and K. A. Kim, "Low-Power Photovoltaic Energy Harvesting With Parallel Differential Power Processing Using a SEPIC," in 2019 IEEE Applied Power Electronics Conference and Exposition (APEC), 2019, pp. 2008-2014.

[7] H. Zhou, J. Zhao, and Y. Han, "PV Balancers: Concept, Architectures, and Realization," IEEE Transactions on Power Electronics, vol. 30, pp. 3479-3487, 2015.

[8] B. V. P. Chong and L. Zhang, "Controller design for integrated PV–converter modules under partial shading conditions," Solar Energy, vol. 92, pp. 123-138, 2013.

[9] M. Veerachary, T. Senjyu, and K. Uezato, "Analytical investigations for maximum power tracking of PV supplied IDB converter," in 2001 IEEE 32nd Annual Power Electronics Specialists Conference (IEEE Cat. No.01CH37230), 2001, vol. 1, pp. 205–209

[10] P. Motsoeneng, J. Bamukunde, and S. Chowdhury, "Comparison of Perturb & Observe and Hill Climbing MPPT Schemes for PV Plant Under Cloud Cover and Varying Load," in 2019 10th International Renewable Energy Congress (IREC), 2019, pp. 1-6.

[11] A. Saleh, K. S. F. Azmi, T. Hardianto, and W. Hadi, "Comparison of MPPT Fuzzy Logic Controller Based on Perturb and Observe (P&O) and Incremental Conductance (InC) Algorithm On Buck-Boost Converter," in 2018 2nd International Conference on Electrical Engineering and Informatics (ICon EEI), 2018, pp. 154-158.

7 Appendix

Coefficients of transfer functions in **section 3.1** are expressed as:

$$b_3 = CC_nL,\ b_2 = \frac{C_nL}{R_{pv2}} + CL(1-K)\left(\frac{(1-K)}{R_{pv1}} - \frac{K}{R_{pv2}}\right)$$
$$b_1 = C_n + CK + \frac{L(1-K)}{R_{pv2}}\left(\frac{(1-K)}{R_{pv1}} - \frac{K}{R_{pv2}}\right),\ b_0 = \frac{(1-K)^2}{R_{pv1}} + \frac{K^2}{R_{pv2}} \quad (1)$$
$$a_5 = (CL)^2C_n\ ,\ a_4 = CC_nL^2\left(\frac{1}{R_{pv1}} + \frac{1}{R_{pv2}}\right)$$
$$a_3 = C_nL\left(2C + \frac{L}{R_{pv1}R_{pv2}}\right)$$
$$a_2 = L(C_n + CK^2 + C(LK)^2)\left(\frac{1}{R_{pv1}} + \frac{1}{R_{pv2}}\right)$$
$$a_1 = C_n + (K^2 + (1-K)^2)\left(C + \frac{L}{R_{pv1}R_{pv2}}\right), a_0 = \frac{(1-K)^2}{R_{pv1}} + \frac{K^2}{R_{pv2}} \quad (2)$$
$$d_3 = CC_nL\ ,\ \ d_2 = \frac{C_nL}{R_{pv1}} + CLK\left(\frac{K}{R_{pv2}} - \frac{(1-K)}{R_{pv1}}\right)$$
$$d_1 = C_n + C(1-K) + \frac{LK}{R_{pv1}}\left(\frac{K}{R_{pv2}} - \frac{(1-K)}{R_{pv1}}\right)$$
$$d_0 = \frac{(1-K)^2}{R_{pv1}} + \frac{K^2}{R_{pv2}} \quad (3)$$

Note that in the above equations (1) to (3), the passive components of the BCC are chosen such that C_1=C_2=C and L_1=L_2=L. V_T is the sum of the PV terminal voltages ($V_T = V_{PV1} + V_{PV2}$). R_{pv1} and R_{pv2} are both obtained by taking the gradient of the I-V characteristics curve of PV_1 and PV_2 modules respectively at a particular point and change with the operating point.